Rapid Communications

Structure determination of the Si(111)-$\sqrt{7} \times \sqrt{3}$-In atomic-layer superconductor

Tetsuroh Shirasawa,[1,*] Shunsuke Yoshizawa,[2] Toshio Takahashi,[3] and Takashi Uchihashi[4]

[1]*National Metrology Institute of Japan (NMIJ), National Institute of Advanced Industrial Science and Technology (AIST), 1-1-1 Higashi, Tsukuba, Ibaraki 305-8565, Japan*

[2]*Research Center for Advanced Measurement and Characterization, National Institute for Materials Science (NIMS), 1-2-1 Sengen, Tsukuba, Ibaraki 305-0047, Japan*

[3]*Department of Physics, Tokyo Gakugei University, 4-1-1 Nukuikita-machi, Koganei, Tokyo 184-8501, Japan*

[4]*International Center for Materials Nanoarchitectonics (MANA), National Institute for Materials Science (NIMS), 1-1 Namiki, Tsukuba, Ibaraki 305-0044, Japan*

(Received 6 December 2018; published 7 March 2019)

The atomic structure of a superconducting atomic sheet of indium grown on Si(111) surface, i.e., In/Si(111)-$\sqrt{7} \times \sqrt{3}$, is determined by using surface x-ray diffraction (SXRD) and low-energy electron diffraction (LEED). The structure consists of double layers of In atoms with a rectangular arrangement, verifying a theoretical prediction [J. W. Park and M. H. Kang, Phys. Rev. Lett. **109**, 166102 (2012)]. For the so-called hexagonal phase, which has been considered to be a different $\sqrt{7} \times \sqrt{3}$ structure and to undergo a transition to the $\sqrt{7} \times \sqrt{7}$ structure below 265 K, LEED data indicate that the structural basis is $\sqrt{7} \times \sqrt{7}$ even at room temperature. The SXRD data are well reproduced by single-layer In with the In coverage of 10/7 In atoms per Si surface atom, proposed by a theory [J. W. Park and M. H. Kang, Phys. Rev. Lett. **117**, 116102 (2016)].

DOI: 10.1103/PhysRevB.99.100502

The recent discovery of a variety of atomically thin superconductors, such as chalcogenide compounds [1,2], metal-doped graphene [3,4], and atomically controlled interfaces [5–7], makes the study of two-dimensional (2D) superconductivity an active field of material science [8,9]. A particularly interesting class of 2D superconductor is epitaxial metal monolayers grown on semiconductor surfaces [10–14]. It seemed that such a monolayer metal was not a likely candidate for a 2D superconductor, because generally it forms a peculiar atomic arrangement and electronic states distinct from the bulk metal due to a strong interaction with the substrate. However, the discovery of superconductivity of the Si(111)-$\sqrt{7} \times \sqrt{3}$-In structure, an indium atomic layer on Si(111) substrate, broke this preconception [10,15,16]. The finding and its unique properties [17–21] will significantly expand the realm of superconductivity research. For example, in such a surface superconductor, the space inversion symmetry is inherently broken at the interface, usually leading to the Rashba effect [22]. Superconductivity with the Rashba spin splitting can be a platform for studying exotic phenomena such as giant critical magnetic field [23], Cooper pairing with a mixture of spin singlet and spin triplet [24], and topological superconductivity [25]. To study the fascinating physics in detail, precise information about atomic structure is indispensable.

The atomic structure of Si(111)-$\sqrt{7} \times \sqrt{3}$-In remains to be clarified possibly due to the following complexity. Deposition of In atoms on the Si(111) surface leads to various structures depending on the coverage and annealing procedure [26,27]. Among them, three distinct $\sqrt{7} \times \sqrt{3}$ structures were identified by scanning tunneling microscopy (STM) observations, which have been called rectangular phase (hereafter $\sqrt{7} \times \sqrt{3}$-rect), hexagonal phase (hereafter $\sqrt{7} \times \sqrt{3}$-hex), and striped phase [26–29], though discrepancies still remain in the interpretation [28,30].

For $\sqrt{7} \times \sqrt{3}$-rect, the In atoms are considered to form a quasirectangular array with $\sqrt{7} \times \sqrt{3}$ periodicity with respect to the Si(111)-1×1 lattice. Initially, it was assumed to be single-layer In with a coverage of 1.2 ML (1 ML is defined as one In atom per one Si surface atom) [26,27], and later on a double-layer model with the coverage of 2.4 ML [Fig. 1(a)] was suggested by first-principles calculations [31]. The double-layer model well reproduces the 2D free-electron-like parabolic band dispersions and circular Fermi surfaces observed by angle-resolved photoemission spectroscopy experiments [32]. However, the atomic structure has not been verified experimentally.

For $\sqrt{7} \times \sqrt{3}$-hex, first a single-layer model with In coverage of 1.0 ML was proposed [33], and then Park and Kang proposed a different single-layer model with a coverage of 1.4 ML by using first-principles calculations [34]. They also proposed a structure model of $\sqrt{7} \times \sqrt{7}$ [Fig. 1(b)], which has been regarded as the low-temperature phase of $\sqrt{7} \times \sqrt{3}$-hex [35]. The coverage of the $\sqrt{7} \times \sqrt{7}$ model is $10/7 \approx 1.43$ ML, and the atomic structure is very similar to the $\sqrt{7} \times \sqrt{3}$-hex model [36]. Since the surface is unstable under STM observations [35,37], surface diffraction experiments are required to clarify the atomic structure. Recently, a low-energy electron diffraction (LEED) study showed that the structure is identical between the $\sqrt{7} \times \sqrt{3}$-hex and striped phases [38], but the atomic structure has not been determined yet.

In this paper, the atomic structures of $\sqrt{7} \times \sqrt{3}$-rect and $\sqrt{7} \times \sqrt{3}$-hex are studied by using surface x-ray

*t.shirasawa@aist.ac.jp

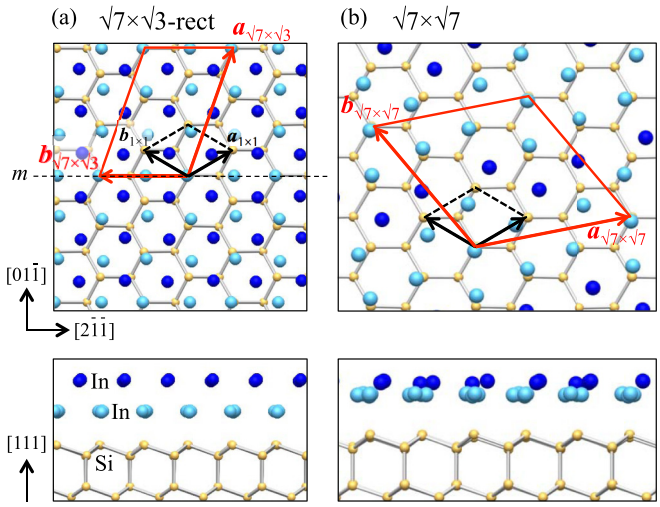

FIG. 1. Structure models of the (a) $\sqrt{7} \times \sqrt{3}$-rect phase [31] and (b) $\sqrt{7} \times \sqrt{7}$ phase [36]. The solid and dashed parallelograms indicate the unit cells of the superstructures and substrate, respectively. In the top views, only the topmost Si bilayer is shown for the substrate. In (a), the horizontal dashed line m indicates a mirror plan.

diffraction (SXRD) and LEED. For $\sqrt{7} \times \sqrt{3}$-rect, the quantitative SXRD and LEED analyses fully verify the double-layer model. For $\sqrt{7} \times \sqrt{3}$-hex, LEED observations suggest that the structural basis is essentially identical to the $\sqrt{7} \times \sqrt{7}$

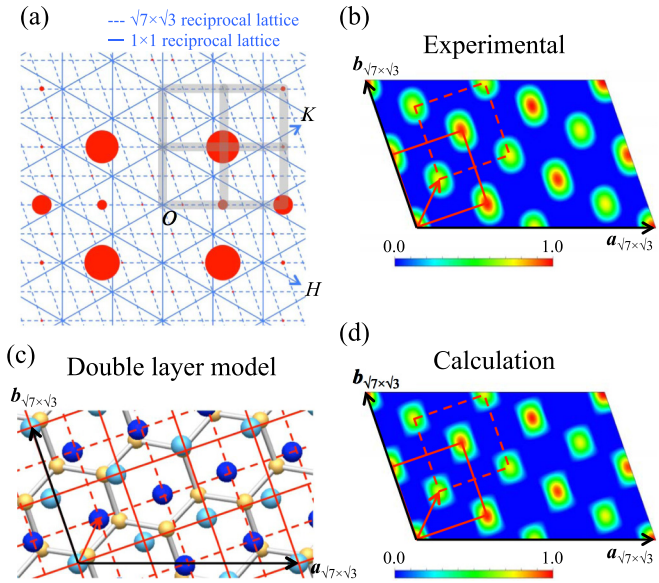

FIG. 2. (a) In-plane SXRD intensity distribution (42 fractional order rods) of $\sqrt{7} \times \sqrt{3}$-rect. The radius of a circle is proportional to the intensity. The bold grid indicates the rectangular lattice in the reciprocal space, which is the counterpart representation of the rectangular array of In. (b) 2D Patterson map constructed from (a). The solid and dashed rectangles represent the array of In atoms in each layer. (c) The top view of the double-layer model [Fig. 1(a)]. The rectangular array of In atoms in each layer is indicated by the solid and dashed rectangles. (d) 2D Patterson map calculated for the double-layer model. In the calculation, the same fractional-order rods as in (a) are used.

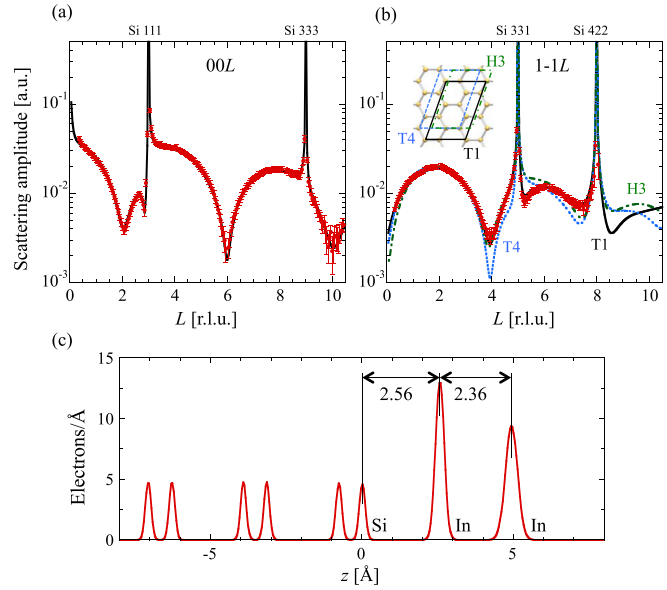

FIG. 3. (a) Specular CTR and (b) nonspecular CTR of $\sqrt{7} \times \sqrt{3}$-rect. The inset in (b) shows three candidates for the location of the $\sqrt{7} \times \sqrt{3}$ unit cell. (c) The projected electron density profile of $\sqrt{7} \times \sqrt{3}$-rect.

low-temperature phase. The SXRD data are well reproduced by the 10/7-ML model.

Details of the sample preparation, experiment, and analysis are described in the Supplemental Material [39]. The in-plane structure of $\sqrt{7} \times \sqrt{3}$-rect was studied by in-plane SXRD measurements. Figure 2(a) shows the distribution of diffraction intensities of the fractional-order rods at $L = 0.5$, where the reciprocal lattice indices of (HK) rod and L are based on the Si(111)-1 × 1 lattice [see Fig. 1(a)] with $c = 9.407$ Å. The intensity is dominated by the x-ray scattering from the In, because In is a much stronger scatterer than Si and the Si surface is not reconstructed. The intensity is significantly strong at the corners of the rectangular lattice indicated by the bold grid, directly indicating the rectangular array of In atoms. The arrangement is clearly displayed in the 2D Patterson map [Fig. 2(b)], the autocorrelation function of electron density, which was constructed by Fourier transform of the in-plane SXRD intensities. The map shows two kinds of peaks, and each one forms the rectangular lattice (solid and dashed lines). The corner of one rectangle is located at the center of the other one as indicated by the arrow. The rectangular array is consistent with the arrangement of In atoms in the double-layer model, as indicated in Fig. 2(c). Actually, the simulated Patterson map for the double-layer model nicely reproduces the experimental one [Fig. 2(d)].

The interlayer spacing between the In layers, their relative position to the substrate, and the height of the top Si bilayers were studied by x-ray crystal truncation rod (CTR) scattering. The scattering amplitude along the specular $00L$ rod and nonspecular $1-1L$ rod are shown in Figs. 3(a) and 3(b). The data are almost perfectly reproduced by the double-layer model (the R factor is 0.04). The resulting electron density profile projected on the z axis is shown in Fig. 3(c), representing the double peak of In. The In coverage in each

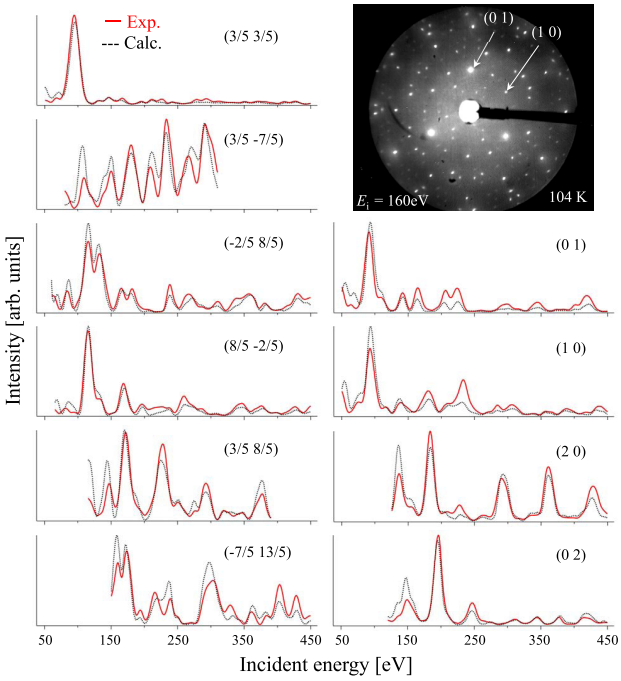

FIG. 4. LEED *I-V* spectra of $\sqrt{7} \times \sqrt{3}$-rect at 104 K. The inset is the LEED pattern.

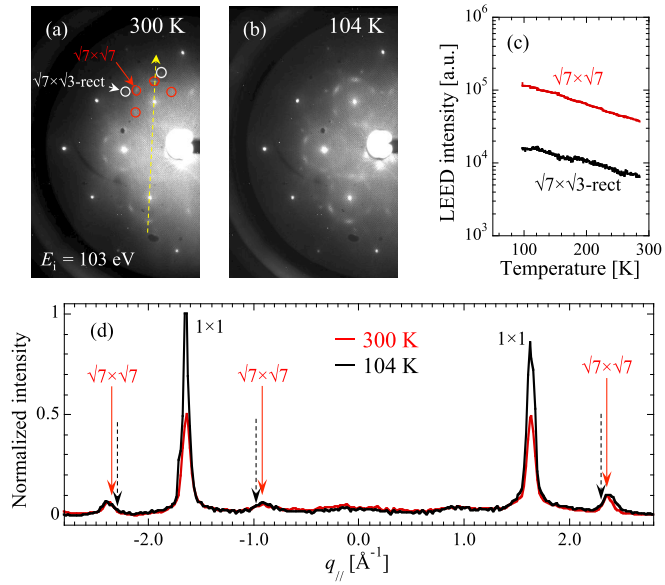

FIG. 5. (a) and (b) LEED patterns observed at 300 K and 104 K for the $\sqrt{7} \times \sqrt{7}$ structure, respectively. (c) Integrated intensities of the streaky $\sqrt{7} \times \sqrt{7}$ spot and $\sqrt{7} \times \sqrt{3}$-rect spot during the cooling. (d) Intensity profile along the dashed arrow in (a). The dashed arrows in (d) indicate the locations of LEED spots expected for $\sqrt{7} \times \sqrt{3}$.

layer, corresponding to the peak area of the electron density profile, is 1.2 ML, in agreement with the double-layer model. The In layers show the broader peaks as compared to the substrate layers, because the In layers are not completely flat but slightly corrugated. The corrugation is larger in the second In layer (the higher layer). For the lateral location of In lattice with respect to the substrate, the possible threefold symmetry sites T1, T4, and H3 were examined as shown in Fig. 3(b). The T1 site is the best fit, consistent with the double-layer model [see Fig. 1(a)].

The atomic coordinates of $\sqrt{7} \times \sqrt{3}$-rect, including the top Si bilayers, was optimized by LEED intensity-voltage (LEED *I-V*) analysis. The LEED patterns were recorded at 104 K to reduce the thermal vibrational effect on the diffraction intensity (Debye-Waller factor), and 33 *I-V* spectra were acquired. All the spectra are well reproduced by the double-layer structure (the Pendry *R* factor is 0.20 [40]). Ten of them are shown in Fig. 4. The optimized atomic coordinates are given in the Supplemental Material with the "cif" file format [41]. The coordinates agree well with those obtained by our first-principles calculations, as shown in Table S1 [39]. The In-In bond lengths range from 3.10 to 3.49 Å and are similar to those in the bulk In, either 3.25 or 3.38 Å. The In-Si bond lengths are either 2.60 or 2.63 Å for the three In atoms located near the atop of the surface Si atoms. The values are close to the sum of covalent radii of 2.5 Å, indicating a strong In-Si interaction. The theoretical study pointed out that the first In layer screens the interfacial interaction and the free-electron-like states are created by the second In layer [36].

Next, the structure of $\sqrt{7} \times \sqrt{3}$-hex was studied. For the sample preparation two procedures are known: one is that In is deposited on the $\sqrt{3} \times \sqrt{3}$ phase (In coverage is 1/3 ML [42]) at room temperature [35], and the other one is that In is deposited on the Si(111)-7 × 7 clean surface at room temperature and then the sample is annealed above 650 K [27,38]. In the former case, $\sqrt{7} \times \sqrt{3}$-hex can cover most of the surface, but it always coexists with a fraction of 2 × 2 [43,44] and/or $\sqrt{7} \times \sqrt{3}$-rect phases. In the latter case, $\sqrt{7} \times \sqrt{3}$-hex coexists with the 4×1 phase [45] (sometimes this $\sqrt{7} \times \sqrt{3}$ has been called the striped phase [27]) and the population of $\sqrt{7} \times \sqrt{3}$-hex is often smaller as compared to the former case. In this study, we adopted the former procedure for reliable structure analysis. The recent LEED study showed that both procedures result in an identical atomic structure [38].

At the nominal In coverage of 1.35 ML [39], the LEED patterns of Figs. 5(a) and 5(b) were observed at 300 and 104 K, respectively. It was reported that $\sqrt{7} \times \sqrt{3}$-hex is transformed to $\sqrt{7} \times \sqrt{7}$ below 265 K [35]. The LEED pattern at 104 K [Fig. 5(b)] shows streaky $\sqrt{7} \times \sqrt{7}$ spots, which is similar to the LEED pattern at 214 K in the previous report [37]. Such a streaky spot appears when the correlation length of the $\sqrt{7} \times \sqrt{7}$ lattice is small (short-range order), as shown in Fig. S3 [39]. In the present study, the streaky spots were observed even at 300 K [Fig. 5(a)], although they were weaker and less streaky. The streaky spots are located on the short-range-order $\sqrt{7} \times \sqrt{7}$ lattice and deviate from the $\sqrt{7} \times \sqrt{3}$ lattice, as shown in the intensity profile of Fig. 5(d). During cooling, the intensity integrated over the streaky spot was increased according to the Debye-Waller factor and did not show an abrupt change [Fig. 5(c)]. These behaviors indicate that a significant structural change did not occur and only the correlation length was increased upon cooling. We note that the LEED patterns contain weak $\sqrt{7} \times \sqrt{3}$ spots as well [Fig. 5(a)]. We confirmed that the spots originate from $\sqrt{7} \times \sqrt{3}$-rect based on their LEED *I-V* spectra.

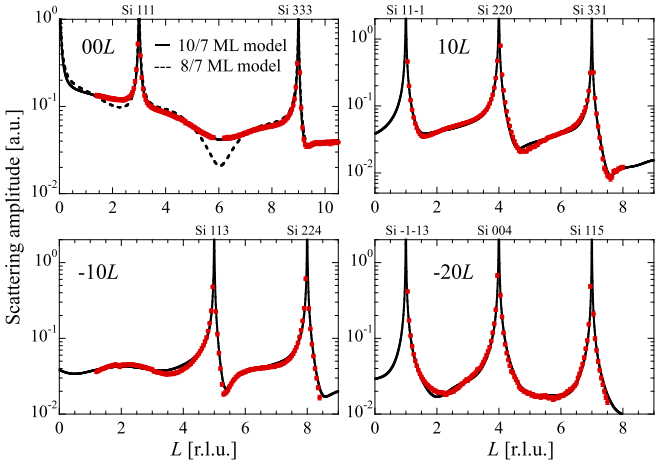

FIG. 6. CTRs of the $\sqrt{7} \times \sqrt{7}$ structure at 300 K. Solid and dashed lines are calculated CTRs for the 10/7 ML model [36] and 8/7 ML model [37], respectively.

The interpretation of the structural change seems inconsistent with the previous reports which assumed the phase transition from $\sqrt{7} \times \sqrt{3}$ to $\sqrt{7} \times \sqrt{7}$ [37,38]. However, according to our examination, the previously reported LEED patterns [31,32] do not accord with the $\sqrt{7} \times \sqrt{3}$ lattice; rather, they coincide with the $\sqrt{7} \times \sqrt{7}$ lattice if short-range order is assumed (see Fig. S4 [39]). Furthermore, we found a good agreement of LEED *I-V* spectra between $\sqrt{7} \times \sqrt{7}$ in the present study and $\sqrt{7} \times \sqrt{3}$-hex in Ref. [38] (see Fig. S5 [39]), demonstrating the structural equivalence. Based on the facts, we suggest that the reported structural change is not a displacive-type phase transition but an order-disorder type crossover originating in an increase of correlation length of $\sqrt{7} \times \sqrt{7}$. This assignment contradicts with the previous STM observations claiming that the $\sqrt{7} \times \sqrt{7}$ structure is formed only below 265 K [28,35,37]. A possible reason for the discrepancy is a STM-induced structural change. This interpretation is supported by the fact that an extrinsic transformation between $\sqrt{7} \times \sqrt{3}$ and $\sqrt{7} \times \sqrt{7}$ occurs during the STM observations [35].

The structure at 300 K was studied by using CTR scattering on the basis of the $\sqrt{7} \times \sqrt{7}$ unit cell. The CTR profiles are shown in Fig. 6. Since we could not obtain a sufficient amount of fractional-order rod data due to the weak signal, we analyzed the $\sqrt{7} \times \sqrt{7}$ structure folded onto the 1×1 unit cell by using the CTR data (integral-order rods). The analysis assumed that all the possible mirrored and rotational domains of $\sqrt{7} \times \sqrt{7}$ coexist within the x-ray interference length (>100 nm) with an identical population, considering the short correlation length of $\sqrt{7} \times \sqrt{7}$. The analysis also took account of the population of $\sqrt{7} \times \sqrt{3}$-rect, which was eventually estimated as $5 \pm 1\%$. We examined two groups for the structure model: the one is shown in Fig. 1(b) whose In coverage is $10/7 \approx 1.43$ ML [36] and the other groups having the coverage of $8/7 \approx 1.14$ ML [37]. As shown in Fig. 6, the 10/7 ML model nicely reproduces the specular 00*L* CTR, which is very sensitive to the coverage and interlayer spacing, while the 8/7 ML models are ruled out. The 10/7 ML model reproduces the nonspecular CTRs as well; the overall *R* factor is 0.05. The optimized atomic coordinates are given in the Supplemental Material with the "cif" file format [46]. The deviation of the atomic positions from the theoretical model is less than 0.1 Å. In the structure, three of ten In atoms protrude by 0.76 Å on average. The mean interlayer spacing between the lower In atoms and top Si layer is 2.61 Å, indicating a strong interaction. According to the theory, the structure hosts the metallic electronic states, but these are not free-electron-like due to the interaction with the substrate [36].

Finally, we discuss the structure of the previously reported superconducting samples. According to the similarities in STM image and sample preparation conditions, we now conclude that the superconducting samples in Ref. [10] and in our previous studies [15,17–21] had the $\sqrt{7} \times \sqrt{3}$-rect double-layer structure. In Ref. [16], the so-called hexagonal phase was reported to show superconductivity below 2.4 K, which was lower than that of the $\sqrt{7} \times \sqrt{3}$-rect phase by 0.4 K. It is rather difficult to identify the structure with the lower T_c, because the sample was identified only by reflection high-energy electron diffraction (RHEED) observations. We point out, however, that on the basis of our careful STM, LEED, and RHEED observations [15,17–21], the sample preparation in Ref. [16] might lead to a mixture of $\sqrt{7} \times \sqrt{3}$-rect, 4×1, and structural defects. Actually, we have frequently observed that T_c is decreased when the $\sqrt{7} \times \sqrt{3}$-rect phase is polluted by other phases and/or structural defects.

In summary, the double-layer model of the Si(111)-$\sqrt{7} \times \sqrt{3}$-In rectangular structure, the superconducting phase, is experimentally verified. For the so-called hexagonal phase, we propose that its structure is based on the $\sqrt{7} \times \sqrt{7}$ lattice with a short-range order. The x-ray CTR scattering analysis indicates that the structure is single-layer In with In coverage of 10/7 ML, proposed by Park and Kang [36].

We are grateful to J. W. Park and M. H. Kang for providing us the atomic coordinates of $\sqrt{7} \times \sqrt{7}$. This work was supported by JSPS Grant-in-Aid for Scientific Research (16H03866 and 26105008). The synchrotron radiation experiments were done at the Photon Factory, KEK (PF-PAC No. 2016G548 and 2015S2-009) and SPring-8 (Proposal No. 2017B1459).

[1] J. T. Ye, Y. J. Zhang, R. Akashi, M. S. Bahramy, R. Arita, and Y. Iwasa, Science **338**, 1193 (2012).

[2] A. W. Tsen, B. Hunt, Y. D. Kim, Z. J. Yuan, S. Jia, R. J. Cava, J. Hone, P. Kim, C. R. Dean, and A. N. Pasupathy, Nat. Phys. **12**, 208 (2015).

[3] B. M. Ludbrook, G. Levy, P. Nigge, M. Zonno, M. Schneider, D. J. Dvorak, C. N. Veenstra, S. Zhdanovich, D. Wong, P. Dosanjh, C. Straßer, A. Stöhr, S. Forti, C. R. Ast, U. Starke, and A. Damascelli, Proc. Natl. Acad. Sci. USA **112**, 11795 (2015).

[4] S. Ichinokura, K. Sugawara, A. Takayama, T. Takahashi, and S. Hasegawa, ACS Nano **10**, 2761 (2016).

[5] N. Reyren, S. Thiel, A. D. Caviglia, L. F. Kourkoutis, G. Hammerl, C. Richter, C. W. Schneider, T. Kopp, A.-S. Rüetschi, D. Jaccard, M. Gabay, D. A. Muller, J.-M. Triscone, and J. Mannhart, Science **317**, 1196 (2007).

[6] A. T. Bollinger, G. Dubuis, J. Yoon, D. Pavuna, J. Misewich, and I. Božović, Nature (London) **472**, 458 (2011).

[7] J.-F. Ge, Z.-L. Liu, C. Liu, C.-L. Gao, D. Qian, Q.-K. Xue, Y. Liu, and J.-F. Jia, Nat. Mater. **14**, 285 (2014).

[8] C. Brun, T. Cren, and D. Roditchev, Supercond. Sci. Technol. **30**, 013003 (2017).

[9] T. Uchihashi, Supercond. Sci. Technol. **30**, 013002 (2017).

[10] T. Zhang, P. Cheng, W.-J. Li, Y.-J. Sun, G. Wang, X.-G. Zhu, K. He, L. Wang, X. Ma, X. Chen, Y. Wang, Y. Liu, H.-Q. Lin, J.-F. Jia, and Q.-K. Xue, Nat. Phys. **6**, 104 (2010).

[11] C. Brun, T. Cren, V. Cherkez, F. Debontridder, S. Pons, D. Fokin, M. C. Tringides, S. Bozhko, L. B. Ioffe, B. L. Altshuler, and D. Roditchev, Nat. Phys. **10**, 444 (2014).

[12] A. V. Matetskiy, S. Ichinokura, L. V. Bondarenko, A. Y. Tupchaya, D. V. Gruznev, A. V. Zotov, A. A. Saranin, R. Hobara, A. Takayama, and S. Hasegawa, Phys. Rev. Lett. **115**, 147003 (2015).

[13] H.-M. Zhang, Y. Sun, W. Li, J.-P. Peng, C.-L. Song, Y. Xing, Q. Zhang, J. Guan, Z. Li, Y. Zhao, S. Ji, L. Wang, K. He, X. Chen, L. Gu, L. Ling, M. Tian, L. Li, X. C. Xie, J. Liu, H. Yang, Q.-K. Xue, J. Wang, and X. Ma, Phys. Rev. Lett. **114**, 107003 (2015).

[14] S. Ichinokura, L. V. Bondarenko, A. Y. Tupchaya, D. V. Gruznev, A. V. Zotov, A. A. Saranin, and S. Hasegawa, 2D Mater. **4**, 025020 (2017).

[15] T. Uchihashi, P. Mishra, M. Aono, and T. Nakayama, Phys. Rev. Lett. **107**, 207001 (2011).

[16] M. Yamada, T. Hirahara, and S. Hasegawa, Phys. Rev. Lett. **110**, 237001 (2013).

[17] T. Uchihashi, P. Mishra, and T. Nakayama, Nanoscale Res. Lett. **8**, 167 (2013).

[18] S. Yoshizawa, H. Kim, T. Kawakami, Y. Nagai, T. Nakayama, X. Hu, Y. Hasegawa, and T. Uchihashi, Phys. Rev. Lett. **113**, 247004 (2014).

[19] T. Uchihashi, Nanotechnology **26**, 344004 (2015).

[20] S. Yoshizawa, H. Kim, Y. Hasegawa, and T. Uchihashi, Phys. Rev. B **92**, 041410 (2015).

[21] S. Yoshizawa, E. Minamitani, S. Vijayaraghavan, P. Mishra, Y. Takagi, T. Yokoyama, H. Oba, J. Nitta, K. Sakamoto, S. Watanabe, T. Nakayama, and T. Uchihashi, Nano Lett. **17**, 2287 (2017).

[22] Y. A. Bychkov and E. I. Rashba, JETP Lett. **39**, 78 (1984).

[23] T. Sekihara, R. Masutomi, and T. Okamoto, Phys. Rev. Lett. **111**, 057005 (2013).

[24] L. P. Gor'kov and E. I. Rashba, Phys. Rev. Lett. **87**, 037004 (2001).

[25] S. Fujimoto, Phys. Rev. B **77**, 220501 (2008).

[26] J. Kraft, S. Surnev, and F. Netzer, Surf. Sci. **340**, 36 (1995).

[27] J. Kraft, M. G. Ramsey, and F. P. Netzer, Phys. Rev. B **55**, 5384 (1997).

[28] D. Shin, J. Woo, Y. Jeon, H. Shim, and G. Lee, J. Korean Phys. Soc. **67**, 1192 (2015).

[29] K. Iwata, S. Yamazaki, Y. Tani, and Y. Sugimoto, Appl. Phys. Express **6**, 055201 (2013).

[30] T. Suzuki, J. Lawrence, M. Walker, J. M. Morbec, P. Blowey, K. Yagyu, P. Kratzer, and G. Costantini, Phys. Rev. B **96**, 035412 (2017).

[31] J. W. Park and M. H. Kang, Phys. Rev. Lett. **109**, 166102 (2012).

[32] E. Rotenberg, H. Koh, K. Rossnagel, H. W. Yeom, J. Schäfer, B. Krenzer, M. P. Rocha, and S. D. Kevan, Phys. Rev. Lett. **91**, 246404 (2003).

[33] K. Uchida and A. Oshiyama, Phys. Rev. B **87**, 165433 (2013).

[34] J. W. Park and M. H. Kang, Phys. Rev. B **92**, 045306 (2015).

[35] A. A. Saranin, A. V. Zotov, M. Kishida, Y. Murata, S. Honda, M. Katayama, K. Oura, D. V. Gruznev, A. Visikovskiy, and H. Tochihara, Phys. Rev. B **74**, 035436 (2006).

[36] J. W. Park and M. H. Kang, Phys. Rev. Lett. **117**, 116102 (2016).

[37] A. Mihalyuk, A. Alekseev, C. Hsing, C. Wei, D. Gruznev, L. Bondarenko, A. Matetskiy, A. Tupchaya, A. Zotov, and A. Saranin, Surf. Sci. **649**, 14 (2016).

[38] S. Terakawa, S. Hatta, H. Okuyama, and T. Aruga, J. Phys.: Condens. Matter **30**, 365002 (2018).

[39] See Supplemental Material at http://link.aps.org/supplemental/10.1103/PhysRevB.99.100502 for the details of the experiment, analysis, and comparison of the optimized atomic coordinates of $\sqrt{7} \times \sqrt{3}$-rect between LEED *I-V* and DFT, and examination of previous LEED studies.

[40] J. B. Pendry, J. Phys. C: Solid State Phys. **13**, 937 (1980).

[41] See Supplemental Material at http://link.aps.org/supplemental/10.1103/PhysRevB.99.100502 for the determined atomic coordinates of $\sqrt{7} \times \sqrt{3}$-rect.

[42] S. Mizuno, Y. O. Mizuno, and H. Tochihara, Phys. Rev. B **67**, 195410 (2003).

[43] J. P. Chou, C. M. Wei, Y. L. Wang, D. V. Gruznev, L. V. Bondarenko, A. V. Matetskiy, A. Y. Tupchaya, A. V. Zotov, and A. A. Saranin, Phys. Rev. B **89**, 155310 (2014).

[44] S. G. Kwon and M. H. Kang, Phys. Rev. B **89**, 165304 (2014).

[45] O. Bunk, G. Falkenberg, J. H. Zeysing, L. Lottermoser, R. L. Johnson, M. Nielsen, F. Berg-Rasmussen, J. Baker, and R. Feidenhans'l, Phys. Rev. B **59**, 12228 (1999).

[46] See Supplemental Material at http://link.aps.org/supplemental/10.1103/PhysRevB.99.100502 for the determined atomic coordinates of $\sqrt{7} \times \sqrt{7}$.